An End-to-End Framework for the Additive Manufacture of Optimized Tubular Structures

JUN YE[1,2], PINELOPI KYVELOU[1], FILIPPO GILARDI[3], HONGJIA LU[4], MATTHEW GILBERT[4], AND LEROY GARDNER[1]

[1]Department of Civil and Environmental Engineering, Imperial College London, London SW7 2AZ, U.K.
[2]College of Civil Engineering and Architecture, Zhejiang University, Hangzhou 310058, China
[3]MX3D, 1014 BK Amsterdam, The Netherlands
[4]Department of Civil and Structural Engineering, The University of Sheffield, Sheffield S1 3JD, U.K.

Corresponding author: Pinelopi Kyvelou (pinelopi.kyvelou11@imperial.ac.uk)

ABSTRACT Although additive manufacturing (AM) has been maturing for some years, it has only recently started to capture the interest of the cost-sensitive construction industry. The research presented herein is seeking to integrate AM into the construction sector through the establishment of an automated end-to-end framework for the generation of high-performance AM structures, combining sophisticated optimization techniques with cutting edge AM methods. Trusses of tubular cross-section subjected to different load cases have been selected as the demonstrators of the proposed framework. Optimization studies, featuring numerical layout and geometry optimization techniques, are employed to obtain the topology of the examined structures, accounting for practical and manufacturing constraints. Cross-section optimization is subsequently undertaken, followed by a series of geometric operations for the design of free-form joints connecting the optimized members. Solid models of the optimized designs are then exported for wire arc additive manufacturing (WAAM). Following determination of the optimal printing sequence, the trusses are printed and inspected. The efficiency of the optimized designs has been assessed by means of finite element modelling and compared against equivalent conventional designs. Design efficiency (reflected in the capacity-to-mass ratios) was at least doubled for all optimized trusses (when compared to their equivalent reference designs), demonstrating the effectiveness of the proposed optimization framework.

INDEX TERMS Additive manufacturing, end-to-end framework, free-form joints, geometry optimization, layout optimization, optimized trusses.

I. INTRODUCTION

Additive manufacturing (AM), also known as 3D printing, has already gained traction in the aerospace, automotive, biomedical and other engineering industries, owing to its numerous benefits. These include the ability to attain high efficiency in terms of material utilisation, opportunities for high degrees of customisation and the elimination of the need for tooling or machining. However, although AM methods have been maturing over the past few decades, it is only recently that this technology has started to capture the interest of the construction industry, where structural elements tend

to be larger in scale and beyond the scope of early 3D printing technologies. Furthermore, the construction industry is often cost-sensitive, and early AM parts tended to be prohibitively expensive [1]. This changed with the introduction of wire arc additive manufacturing (WAAM), which allows high deposition rates, involves low material and equipment costs and can produce parts of virtually unlimited size and with good structural integrity [2]–[5]. A demonstration of this is the world's first metal 3D printed bridge [6], manufactured by MX3D [7], using their proprietary multi-axis robotic WAAM technology – see Figure 1. The more widespread adoption of AM could significantly increase the degree of automation, improve workplace safety and increase overall construction efficiency, bringing about a step change in the

The associate editor coordinating the review of this manuscript and approving it for publication was Mauro Gaggero .

FIGURE 1. (a) WAAM robotic facility and (b) WAAM of the MX3D bridge.

construction sector. Furthermore, the potential for increased geometric freedom and the use of different base materials offer the potential to produce structural parts formed with intricate customised geometries, potentially leading to more optimized, structurally efficient and aesthetically pleasing structures.

Structural optimization methods can be used to generate highly material-efficient structures. However, these structures can be geometrically complex and hence difficult to manufacture via conventional means. The ability to fabricate geometrically complex forms using AM opens up opportunities to unleash the true potential of structural optimization. Relevant optimization methods include continuum (mesh based) topology optimization [8] and discrete (ground structure based) layout optimization [3]. The continuum approach has now been widely applied to the design of AM components. However, the continuum approach is not well-suited to problems where the optimized structure will occupy only a very small fraction of the available design space, as is commonly the case for civil engineering structures. Also, labour intensive post-processing may be required to generate an AM-ready physical model. On the other hand, layout optimization performs well for problems where the optimized

structure occupies only a small proportion of the available design domain; in such cases, frame structures can be identified directly, without the need for labour intensive post-processing, and computationally efficient adaptive solution methods are available [9]. Methods have been developed to automatically transform the structural layout obtained using this approach into a model suitable for building using powder bed fusion [10], with geometric refinement [11] and with overhangs [12]. However, application of layout optimization to the design of structures fabricated via WAAM has to date received scant attention.

The research presented herein seeks to combine sophisticated optimization techniques with cutting edge AM methods, with a view to establish an automated end-to-end framework for the generation of WAAM optimized structures. Trusses formed of tubular cross-sections subjected to different load cases have been selected as demonstrators of the proposed framework. Optimization studies, featuring numerical layout and geometry optimization techniques, are employed to obtain a 'line structure' output for the given problem considering practical and manufacturing constraints. Cross-section optimization is then carried out, followed by a series of geometrical operations for the design of free-form joints connecting the optimized members. Solid models of the finalised truss designs are then generated and exported as STL files to be fed into the WAAM specific CAM software tool for AM. The performance of the optimized trusses is assessed via finite element modelling and comparisons are drawn with equivalent conventional designs. Finally, the optimum build-up sequence for the trusses is determined and the trusses are printed and inspected.
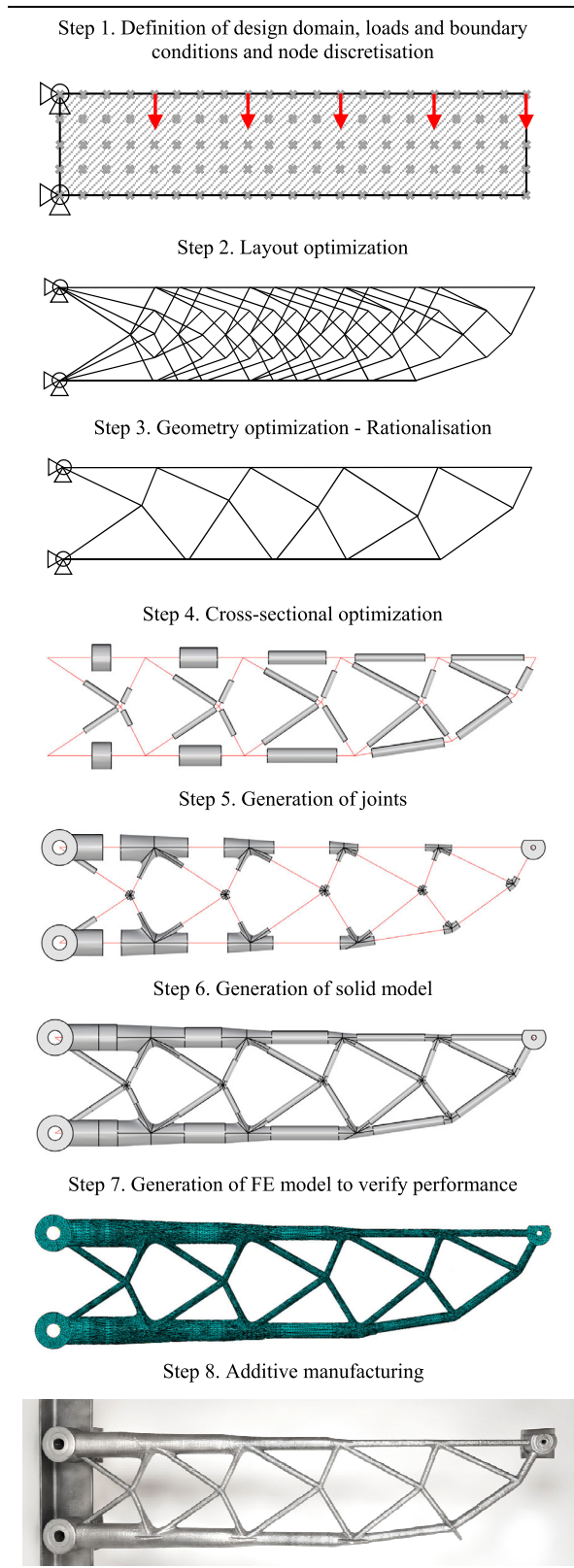
II. SUMMARY OF KEY STEPS IN THE PROPOSED FRAMEWORK

The framework presented in Table 1 is proposed for the production of optimized AM tubular trusses. Implementation of the steps indicated below is described in the following sections.

III. LAYOUT AND GEOMETRY OPTIMIZATION

The first three steps of the design framework introduced in Section II are described in this section. First, the design requirements and available design domain should be established. Layout optimization is then undertaken to determine the optimal layout (or 'topology') of the members, described by a line model. Finally, geometry optimization is carried out to rationalise the obtained solution, simplifying and hence improving the derived line model.

Generic trusses subjected to typical load levels for building structures were selected as demonstrators of the proposed framework; three boundary conditions were considered: simply supported, propped cantilever and cantilever. The boundary conditions and load cases considered for each truss, as well as the 400 × 2000 mm design domain, are shown in Figure 2.

TABLE 1. Key steps of proposed framework.

Step 1. Definition of design domain, loads and boundary conditions and node discretisation

Step 2. Layout optimization

Step 3. Geometry optimization - Rationalisation

Step 4. Cross-sectional optimization

Step 5. Generation of joints

Step 6. Generation of solid model

Step 7. Generation of FE model to verify performance

Step 8. Additive manufacturing

The mechanical properties assigned to the WAAM material for the optimization studies were obtained based on a comprehensive series of tensile material tests performed on

coupons cut from flat plates printed using the same feedstock material and printing parameters as the trusses [13]. In the conducted study [13], the influence of the undulating surface, which is inherent to the WAAM process, on the material response of WAAM carbon steel was investigated by testing machined and as-built coupons. The degree of material anisotropy, which has been found to be significant for WAAM stainless steel [14]–[17], was also investigated by testing coupons produced at 0°, 30°, 45°, 60° and 90° to the print layer orientation, but was found not to be significant in the studied material. The negative influence of the surface undulations, inherent to the WAAM process, was unveiled by comparisons between the mechanical properties of the as-built and machined (i.e. smooth) coupons [13], [18]. For the conducted optimization and FE studies reported herein, the mechanical properties of the as-built coupons produced at a 90° angle to the print layer orientation were employed, with the elastic modulus, yield stress and ultimate tensile stress taken as $E = 201.2$ GPa, $f_y = 345$ MPa and $f_u = 458$ MPa, respectively.

Finally, it should be mentioned that the optimization studies undertaken were carried out with respect to the in-plane capacity of the beams, assuming the occurrence of no out-of-plane deformations. Such conditions are frequently met in typical structures, such as floor systems or roof systems, where sufficient lateral bracing is provided to prevent out-of-plane deformation of the supporting members. Note that the same boundary conditions were used in the conducted finite element analyses (by applying lateral restraints along the compression chord of the trusses – see Section VI) and will be also employed during physical testing of the trusses.

A. LAYOUT OPTIMIZATION

The first step in the proposed optimization process is layout optimization. Firstly, the design domain, boundary conditions and target design loads P_i (see Section VI) for i different load cases (with $i = 1, \ldots, 5$) are specified – see Figure 2. A 'ground structure' is then generated, comprising a grid of nodes whose number is sufficient for the determination of the optimum volume of the examined structure. The connections between the nodes describe the potential truss member positions; the generated node grids are illustrated in Figure 2. Finally, a solution of the underlying problem is sought.

Both elastic and plastic formulations for layout optimization studies have been explored by the research community. The main shortcoming of the standard elastic formulation, where the minimum compliance solution is sought, is that the stiffness matrix may become singular due to the presence of members with cross-sectional areas almost equal to zero. In contrast, the plastic layout optimization formulation involves the use of a force equilibrium matrix and thus, does not suffer from this problem. This latter formulation was therefore employed for the truss designs examined herein.

For a pin-jointed truss structure comprising n nodes, m axially loaded members and M load cases, the plastic layout optimization formulation, designed to determine the
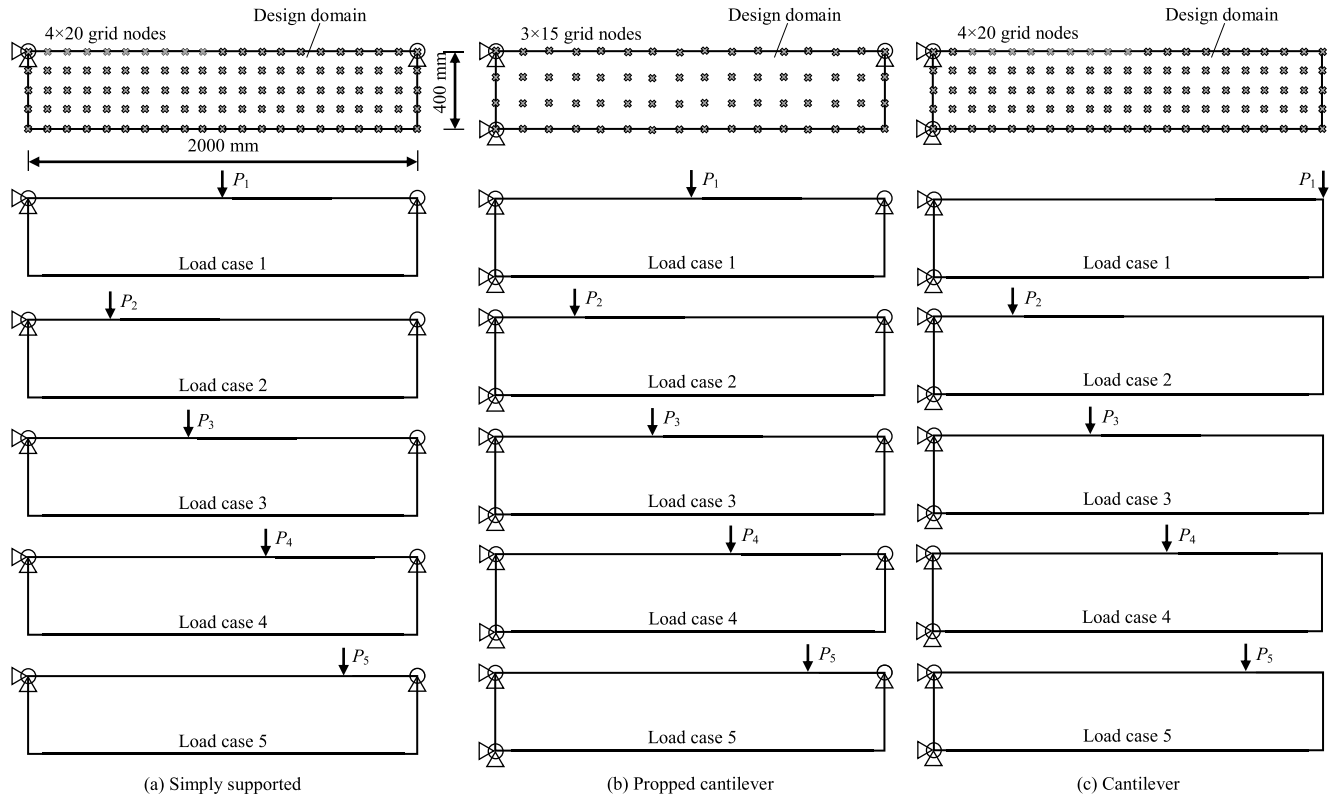
FIGURE 2. Design domain, boundary conditions and load cases for (a) simply supported, (b) propped cantilever and (c) cantilever trusses.

minimum volume of material that satisfies force equilibrium and limiting stress criteria, can be written as follows:

$$\min V = L^{\mathrm{T}} A \tag{1}$$

$$\text{subject to: } Bq^{\delta} = \mathrm{f}^{\delta}, \quad \delta = 1, \ldots, \mathrm{M} \tag{2}$$

and

$$
\left.
\begin{array}{l}
A_{\mathrm{i}} \geq \left\{ \dfrac{q_{\mathrm{i}}}{f_{\mathrm{yi}}^{+}} \right\}^{\delta} \\[3mm]
A_{\mathrm{i}} \geq \left\{ -\dfrac{q_{\mathrm{i}}}{f_{\mathrm{yi}}^{-}} \right\}^{\delta} \\[3mm]
A_{\mathrm{i}} \geq 0
\end{array}
\right\} \quad \delta = 1, \ldots, \mathrm{M}; \ i = 1, \ldots, \mathrm{m} \tag{3}
$$

where V is the total volume of structural material, $L^{\mathrm{T}} = \{L_1, L_2, \ldots, L_{\mathrm{m}}\}$ and $A^{\mathrm{T}} = \{A_1, A_2, \ldots, A_{\mathrm{m}}\}$ are the vectors of the lengths and cross-sectional areas of the members respectively and B is a nodal equilibrium matrix of size $3n \times 2m$, $q^{\mathrm{T}} = \{q_1, q_2, \ldots, q_{\mathrm{m}}\}$ where q_{i} is the internal force in member i. It should be noted that for any active member in the optimum structure, the internal force can be either tensile or compressive (i.e. $q_{\mathrm{i}} > 0$ for a tensile force and $q_{\mathrm{i}} < 0$ for a compressive force). Finally, $f^{\mathrm{T}} = \{f_1^x, f_1^y, f_1^z, \ldots, f_i^x, f_i^y, f_i^z, \ldots, f_n^x, f_n^y, f_n^z\}$ is the nodal force vector where f_{yi}^{+} and f_{yi}^{-} are the limiting tensile and compressive stresses respectively, while δ is used to denote the load case index of M load cases.

This is a linear programming problem that can be solved efficiently using modern interior-point solvers. For a given nodal discretisation, a globally optimal solution is guaranteed while use of the adaptive 'member adding' technique [9] can significantly improve computational efficiency, with no effect on the optimality of the obtained solution.

B. GEOMETRY OPTIMIZATION – RATIONALISATION

It is well known that the outcome structures obtained from a standard layout optimization with a relatively refined ground structure can be complex in form, leading to impractical designs (e.g. featuring members with very small cross-sections or with a very high number of intersections). Seeking to address this issue, geometry optimization can be used in a post-processing step to rationalise the obtained solutions [11], [12]. This technique has been observed to both simplify and improve the optimality of the solutions and involves adjusting the positions of active nodes and merging nodes that are in close proximity to one another.

C. IMPLEMENTATION

The employed layout and geometry optimization formulations were made available by LimitState through the 'Peregrine' plugin for the Rhinoceros-based geometric modelling tool Grasshopper [19], providing a powerful parametric modelling environment for users. A typical example of the
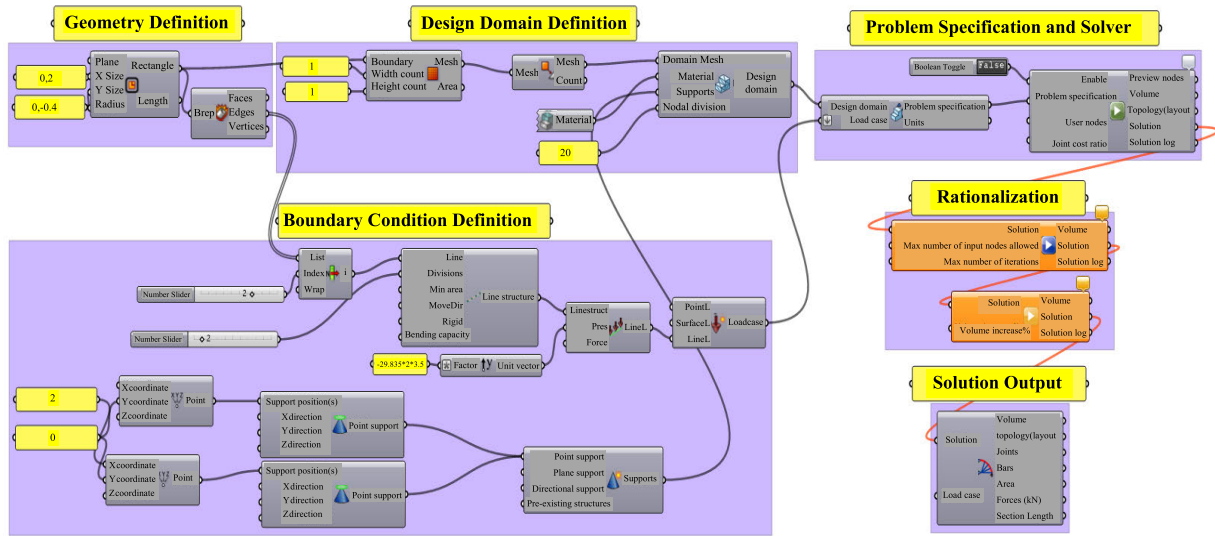
FIGURE 3. Grasshopper plugin workflow employing both layout and geometry optimization.

components used in the workflow is shown in Figure 3, while the resulting line models for the optimized demonstrator trusses (following layout and geometry optimization) are presented in Figure 4.

IV. CROSS-SECTIONAL OPTIMIZATION

Following determination of the optimized topology for the demonstrator trusses, cross-sectional optimization can be undertaken to define the optimal cross-sectional proportions of all truss members, ensuring they are fully stressed and, therefore, fully utilised.

A. DESIGN OF TUBULAR MEMBERS
Members of circular hollow section (CHS) were selected for the optimized trusses since, for a given volume of material, they have larger radii of gyration than solid cross-sections and, thus, higher flexural buckling resistances. However, the use of relatively slender, thin-walled CHS means that local buckling might be significant [20]–[23].

The ultimate compressive capacity of a CHS member with a non-slender (Class 1-3) cross-section N_u can be determined according to EN 1993-1-1 [24] from:

$$N_u = \chi A f_y \tag{4}$$

where A is the cross-sectional area, f_y is the yield strength and χ is the reduction factor for flexural buckling, given by:

$$\chi = \frac{1}{\Phi + \sqrt{\Phi^2 - \bar{\lambda}^2}} \leq 1.0 \tag{5}$$

with

$$\Phi = 0.5 \left[1 + \alpha \left(\bar{\lambda} - 0.2 \right) + \bar{\lambda}^2 \right] \tag{6}$$

in which α is an imperfection factor and $\bar{\lambda}$ is the non-dimensional member slenderness, defined as:

$$\bar{\lambda} = \sqrt{\frac{f_y}{\sigma_F}} \tag{7}$$

where σ_F is the elastic flexural buckling stress given, for a pin-ended member, by:

$$\sigma_F = \frac{\pi^2 E I}{A L^2} \tag{8}$$

where E is the elastic modulus, I is the second moment of area, A is the cross-sectional area and L is the length of the member. The value of the imperfection factor α was taken equal to 0.21 (i.e. the value assigned to hot-finished tubular cross-section members in EN 1993-1-1 [24], though this assumption requires verification.

Optimum structural solutions can be sought in the region where the average applied axial stress in the member is equal to the local and global buckling stresses [25]. This criterion has been used in the optimization process performed herein to determine the geometric design variables of the optimized CHS members, namely the wall thickness t and external diameter d.

The average axial stress σ_s in a CHS member resulting from an applied axial force N is given approximately by:

$$\sigma_s = \frac{N}{\pi d t} \tag{9}$$

The elastic local buckling stress σ_L of a tubular cross-section can be taken as:

$$\sigma_L = \frac{2E}{\sqrt{3 \left(1 - \nu^2 \right)}} \frac{t}{d} = 1.21 E \frac{t}{d} \tag{10}$$

where $\nu = 0.3$ is the Poisson's ratio. To derive a simple and explicit relationship between the optimized cross-sectional
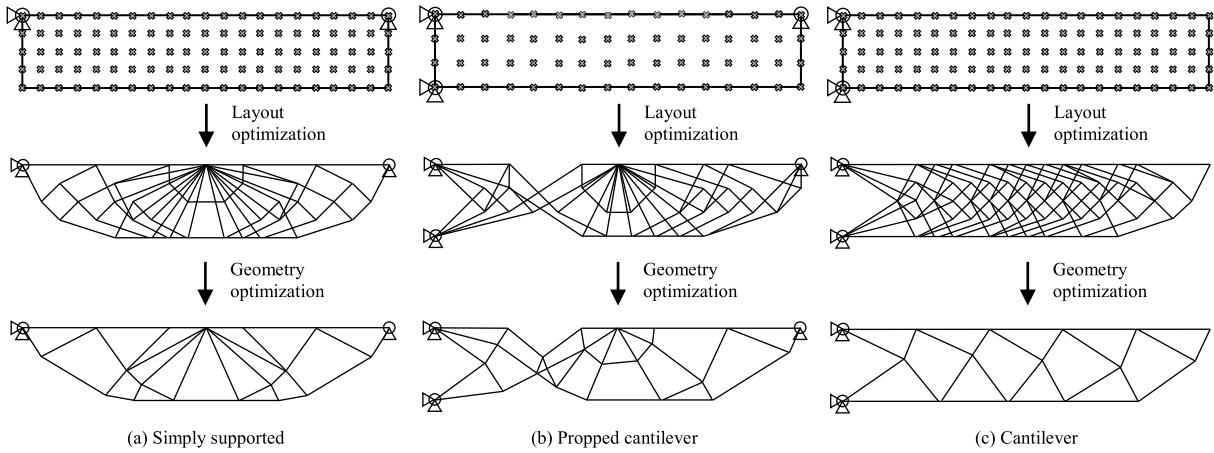
FIGURE 4. (a) Layout and geometry optimization results for: (a) simply supported, (b) propped cantilever, and (c) cantilever trusses.

dimensions and the applied compressive stress given by Equation (9), the following approximations for the key geometric properties were adopted: the second moment of area $I \approx \pi d\, 3t/8$; the cross-sectional area $A \approx \pi dt$; and the radius of gyration $i \approx d/2\sqrt{2}$.

The optimized geometry was therefore determined by equating the applied axial stress σ_s, the local buckling stress σ_L and the flexural buckling stress σ_F:

$$\frac{N}{\pi dt} = 1.21E\frac{t}{d} = \frac{\pi^2 E d^2}{8L^2} \qquad (11)$$

Hence, the diameter d and thickness t of the optimized member can be calculated from:

$$t = 0.513\left(\frac{N}{E}\right)^{1/2} \qquad (12)$$

and

$$d = 0.661\left(\frac{NL^4}{E}\right)^{1/6} \qquad (13)$$

The thickness and diameter of the optimized tubular members should also satisfy constraints pertinent to the WAAM process employed; in this case, the following constraints were applied:

$$t \geq 3.5\ \text{mm} \qquad (14)$$

$$d = \max(2t + 2, 25\ \text{mm}) \qquad (15)$$

Finally, to avoid excessively slender truss members for practical and serviceability purposes, the following member slenderness limitation can also be imposed:

$$\lambda = \frac{L}{i} \geq 150 \qquad (16)$$

B. CROSS-SECTION OPTIMIZATION ALGORITHM

The cross-sections of the truss members can now be optimized using an algorithm developed in MATLAB [26], based on the Optimality Criteria Method, ensuring that all members of the truss topology obtained through the process described

in Section III are fully stressed. For each truss member i of cross-sectional area A_i subjected to M load cases, the maximum value of the ratio $\xi_i^{(k)}$ of the member stress to the allowable stress at iteration k, subjected to all external load cases j, is obtained through:

$$\xi_i^{(k)} = \max_{\delta \in M}\ \left\{\sigma_{i\delta}^{(k)} \big/ \sigma_i\right\} \qquad (17)$$

where σ_i is the allowable stress in the member i (i.e. the buckling stress, determined via Equation (4)). The area A_i of each cross-section can be then optimized through the following equation:

$$A_i^{(k+1)} = \xi_i^{(k)} A_i^{(k)} \qquad (18)$$

A value of $\xi_i^{(k)}$ larger than 1 indicates that the cross-sectional area should increase. The structure is analysed every time the cross-sectional areas of the members are altered. In each iteration, the cross-sectional thickness is calculated using Equations (12) and (14); the diameter is then calculated through Equations (13), (15), (16) and (18).

The optimization process is set to cease when:

$$\left|A_i^{(k+1)} - A_i^{(k)}\right| < \varepsilon \qquad (19)$$

where $\varepsilon = 0.001$.

V. GENERATION OF SOLID MODEL AND JOINTS FOR AM

The topology results obtained via the layout, geometry and cross-sectional optimization processes presented in Sections III and IV are models consisting of line elements with assigned cross-sectional thicknesses and diameters. The processes followed for the generation of the joints between the truss members as well as of the final solid models of the optimized trusses are presented in this section.

The final solid models of the optimized trusses are generated via a Non-Uniform Rational Basis-Splines (NURBS) representation using a Grasshopper plugin [24] developed for Rhino [27]. NURBS are a common means of representing free-form geometries in computer-aided design.

(a)

(b)

(c)

(d)

(e)
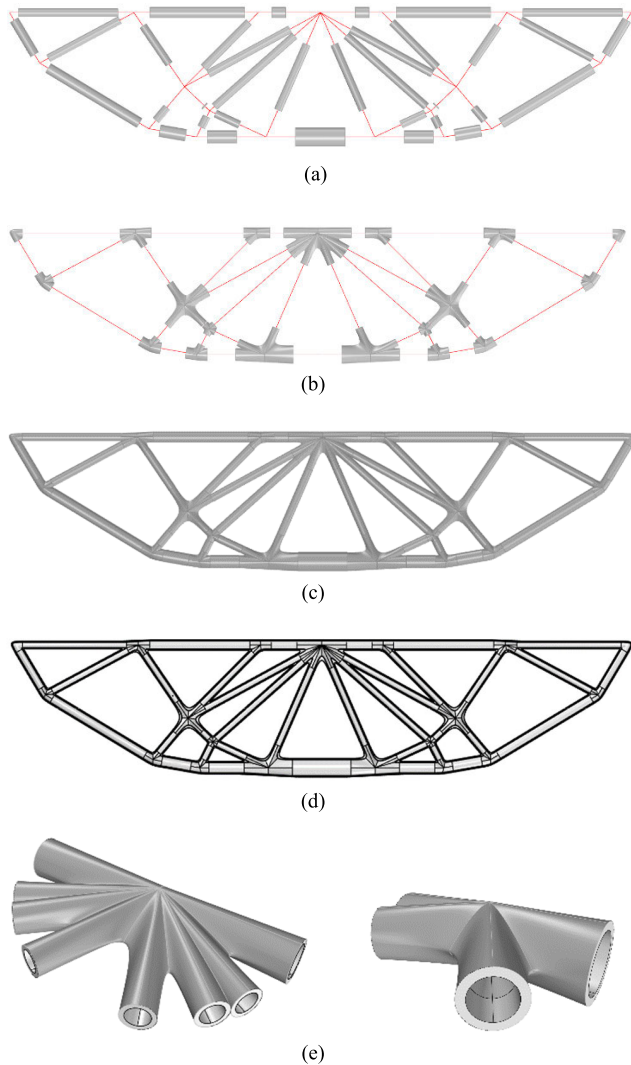
FIGURE 5. Generation of solid model of the simply supported optimized truss: (a) generation of circular members, (b) generation of connections between members, (c) finalised continuum truss, (d) section view of truss and (e) perspective view of typical joints.

Owing to their tubular cross-section profile, the truss members can be generated via two surface layers, with the outer and inner surfaces being determined using the external and internal radii respectively. Each truss member is then created by extruding the external and internal cross-sections along the length of the line elements, as shown in Figure 5(a) for the simply supported truss.

A plugin was developed in Grasshopper [19] for the automatic generation of the connections between the individual circular cross-sections. All circular members are extruded up to a specific distance from the joints and adjacent surfaces are then blended to form smooth tubular joints, as shown in Figure 5(b). The joints and members are then merged to form a closed solid polysurface – see Figure 5(c). Since Rhino is unable to identify the topological relationship between the internal and external polysurface, a cylinder of 1 mm diameter was generated to connect the surfaces using Boolean

Geometry Operations, creating a single watertight surface. The final solid model of the optimized simply supported truss is presented in Figure 5(d) while close-up views of typical joints are shown in Figure 5(e).

Finally, an STL (mesh) file can be generated for AM, while 'SAT', 'STEP' or other standard (Brep) CAD files can be created for input into commercial finite element analysis (FEA) packages, such as ABAQUS [28], which was employed in the present study. Finalised solid models of the optimized simply supported, propped cantilever and cantilever trusses are presented in Figure 6.

(a)

(b)

(c)
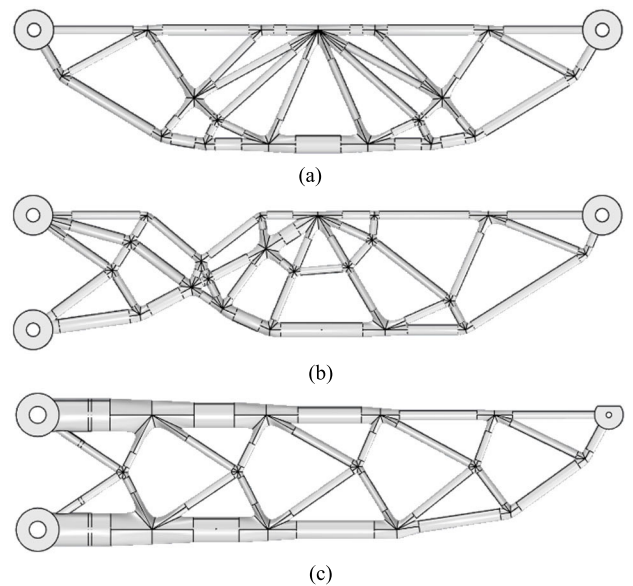
FIGURE 6. Solid models of optimized trusses with the following boundary conditions: (a) simply supported, (b) propped cantilever and (c) cantilever.

VI. NUMERICAL SIMULATION OF OPTIMIZED TRUSSES

In order to evaluate the structural behaviour and capacity of the optimized trusses, geometrically and materially nonlinear finite element (FE) analyses were performed, including initial geometric imperfections (GMNIA) using the FE package ABAQUS [28]. The capacities of equivalent standard universal beam sections, taken as reference designs, were also examined. The key aims of the conducted FE analyses were to: (a) assess the effectiveness of the proposed truss optimization framework and workflow described in the previous sections and (b) investigate the overall efficiency of the developed optimization framework in obtaining designs with improved strength and stiffness and reduced material usage.

A. KEY FEATURES OF FE MODELS
1) ELEMENTS AND MESH SIZE
The solid models composed of NURBS surfaces were firstly transformed to multiple closed polygons which were then meshed in Rhino 3D [27]. The initially generated number of mesh faces was reduced using the 'ReduceMesh' command to achieve increased computational efficiency. In this process,

the quality of the mesh was carefully checked using the 'mesh quality check' command to avoid any overlap between the mesh faces and detect the existence of holes. Finalised mesh models were then changed to a NURBS model in Rhino for export as an 'SAT' file, which can subsequently be imported as a 'Part' in ABAQUS [28].

Here, the general-purpose 10-noded quadrilateral C3D10 solid elements in ABAQUS [28] were chosen for the meshing of the examined 3D printed components. Based on a sensitivity analysis, a mesh size of 10 mm × 10 mm was employed for geometric discretisation of the trusses, with smaller elements used through the thickness of the tubular cross-sections; no significant change in ultimate capacity was observed by further reducing the mesh size.

2) MATERIAL MODELLING
The mechanical properties assigned to the optimized trusses were obtained based on a comprehensive series of tensile material tests performed on coupons cut from flat plates printed using the same feedstock material and printing parameters as the trusses [13]. The obtained stress-strain responses were found to follow similar trends to conventionally manufactured carbon steel [13], [18], [29]; a typical example is shown in Figure 7. Material anisotropy was not found to be pronounced, while both the undulating WAAM surface and coupon thickness were found to be influential on the obtained material properties. Therefore, the material response of the trusses was modelled as isotropic, using the mechanical properties of the as-built coupons produced at a 90° angle to the print layer orientation, with the elastic modulus, yield stress and ultimate tensile stress taken as $E = 201.2$ GPa, $f_y = 345$ MPa and $f_u = 458$ MPa, respectively.

The full stress-strain curves employed in the FE models were derived using the values of E, f_y and f_u stated above, in conjunction with the quad linear constitutive relationship given by Equation (20), comprising four stages: a linear stress-strain response up to the yield stress, a yield plateau and, finally, two linear parts with different slopes corresponding to strain hardening [30].

$$\sigma = \begin{cases} E\varepsilon & \text{for } \varepsilon \leq \varepsilon_y \\ f_y & \text{for } \varepsilon_y < \varepsilon \leq \varepsilon_{sh} \\ f_y + E_{sh}(\varepsilon - \varepsilon_{sh}) & \text{for } \varepsilon_{sh} < \varepsilon \leq C_1\varepsilon_u \\ f_{C_1\varepsilon_u} + \dfrac{f_u - f_{C_1\varepsilon_u}}{\varepsilon_u - C_1\varepsilon_u}(\varepsilon - C_1\varepsilon_u) & \text{for } C_1\varepsilon_u < \varepsilon \leq \varepsilon_u \end{cases}$$

$$\tag{20}$$

In Equation (20), ε and σ are the engineering strain and stress respectively, ε_y is the yield strain, $\varepsilon_u = 0.6(1 - f_y/f_u)$ is the ultimate strain at f_u, $C_1\varepsilon_u$ is the strain at the intersection between the second and third stage of the model, $f_{C_1\varepsilon_u}$ is the stress at $C_1\varepsilon_u$, $\varepsilon_{sh} = 0.1(f_y/f_u) - 0.055$ (but $0.015 \leq \varepsilon_{sh} \leq 0.03$) is the strain hardening strain, $E_{sh} = (f_u - f_y)/[0.4(\varepsilon_u - \varepsilon_{sh})]$ is the strain hardening slope and $C_1 = [\varepsilon_{sh} + 0.25(\varepsilon_u - \varepsilon_{sh})]/\varepsilon_u$ is a material coefficient.
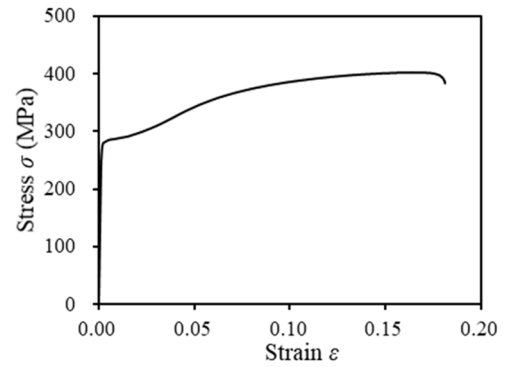

FIGURE 7. Typical stress-strain curve obtained from as-built WAAM carbon steel coupon of 3 mm nominal thickness.

Finally, for input into ABAQUS [28], the engineering stresses and strains were converted into true stresses σ_{true} and true plastic strains ε_{true}^{pl}, according to Equations (21) and (22).

$$\sigma_{true} = \sigma(1 + \varepsilon) \tag{21}$$

$$\varepsilon_{true}^{pl} = \ln(1 + \varepsilon) - \frac{\sigma_{true}}{E} \tag{22}$$

3) BOUNDARY CONDITIONS
The boundary conditions of the modelled demonstrator trusses were simulated by coupling the nodes of both pinholes at the ends of the trusses to a reference point located at the centre of each pinhole (acting as the master node); the degrees of freedom of this reference point were then restrained to reflect the different support configurations (i.e. simply supported, propped cantilever and cantilever). Out-of-plane translational restraints (i.e. U3=0) were imposed along the compressive chord of the trusses – see Figure 8(a), 8(b) and 8(c) for the simply supported, propped cantilever and cantilever trusses respectively.

4) ANALYSIS TYPE
Two types of analysis were carried out to characterise the behaviour of the optimized trusses and verify the optimization process. A first order analysis including an elastic-perfectly plastic material model (MNA) was initially conducted to assess the general accuracy of the optimization framework, with no allowance for strain hardening. Then, a second order analysis including imperfections and material nonlinearity (GMNIA) was undertaken to replicate the true structural behaviour of the optimized trusses. In the GMNIA, the nonlinear material response as determined from the conducted physical tests was assigned to the optimized trusses – see Section VI, while initial geometric imperfections were implemented by scaling the first elastic buckling mode with an amplitude of span/500 (which is typical for spatial trusses). Large deformation effects were taken into consideration by means of a nonlinear geometric analysis, to capture the development of buckling in the members of the examined systems. For both types of analysis, a general static solver with displacement control was employed.
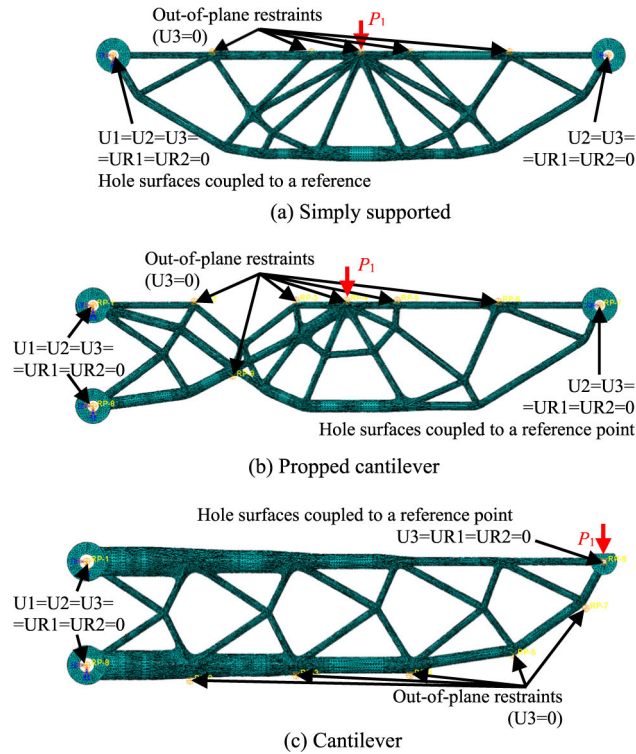
FIGURE 8. Boundary conditions of (a) simply supported, (b) propped cantilever and (c) cantilever trusses.

FIGURE 9. Typical grid structure: (a) isometric view and (b) FE model.
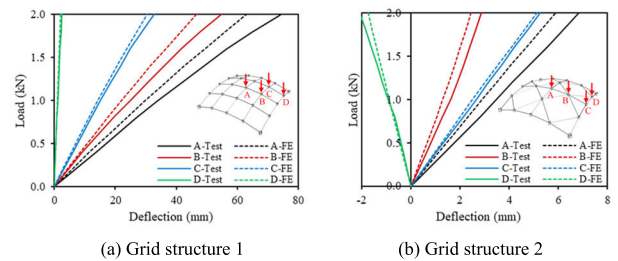
FIGURE 10. Comparisons of load-displacement curves from tests [31] and numerical simulations.

B. VALIDATION OF FE MODELS

The results of an experimental study [31] on two grid structures (one conventional and one optimized), featuring similar cross-sections and connections to those studied herein, were employed to validate the developed FE models. The tested grid structures were 3000 mm × 3000 mm on plan with a height of 600 mm, while the steel grade was Q235, with measured values of Young's modulus, yield stress and ultimate stress of $E = 208$ GPa, $f_y = 342$ MPa and $f_u = 468$ MPa respectively.

The tested grid structures were modelled as described in the previous sub-section, with the boundary conditions appropriately modified to replicate the employed test setup. An isometric view of a typical grid structure, along with the FE model, are illustrated in Figure 9(a) and 9(b) respectively, along with the employed mesh and boundary conditions.

Comparisons between the load-displacement curves obtained from the tests [31] and FE analyses are presented in Figure 10. Good agreement was observed between the results of the tests and the numerical simulations, confirming the capability of the developed FE models to capture the exhibited structural responses.

C. FE ANALYSIS OF OPTIMIZED TRUSSES

Following their validation, the developed FE models were employed to examine the response of the optimized trusses. The defo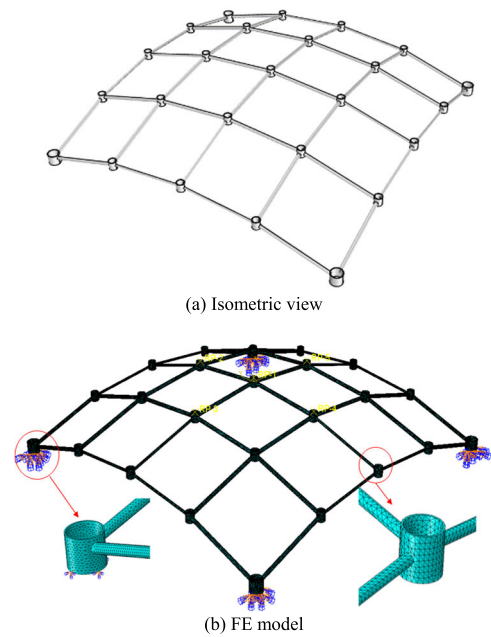rmed shapes and exhibited failure modes, together with the von Mises stress distributions at ultimate load, are shown in Figure 11, while the obtained load-deflection curves are illustrated in Figure 12. All three trusses exhibited significant plasticity, followed by failure due to flexural buckling of the truss members.

The simply supported truss, shown in Figure 11(a), exhibited extensive plasticity in the top and bottom chords prior to failure by flexural buckling within the top chord. The diagonal members remained at relatively lower stress levels since their minimum dimensions were limited by the manufacturing constraints prescribed by Equations (14) and (15). No failure was observed in the free-form joints owing to their increased thickness. The deformed shapes and failure modes of the FE models of the propped cantilever and cantilever trusses are presented in Figure 11(b) and 11(c) respectively. Failure of the propped cantilever was triggered by out-of-plane buckling of the top chord and of the diagonal member adjacent to the loading position while, for the cantilever truss, buckling developed in two members of the compression chord, near to the cantilever tip.
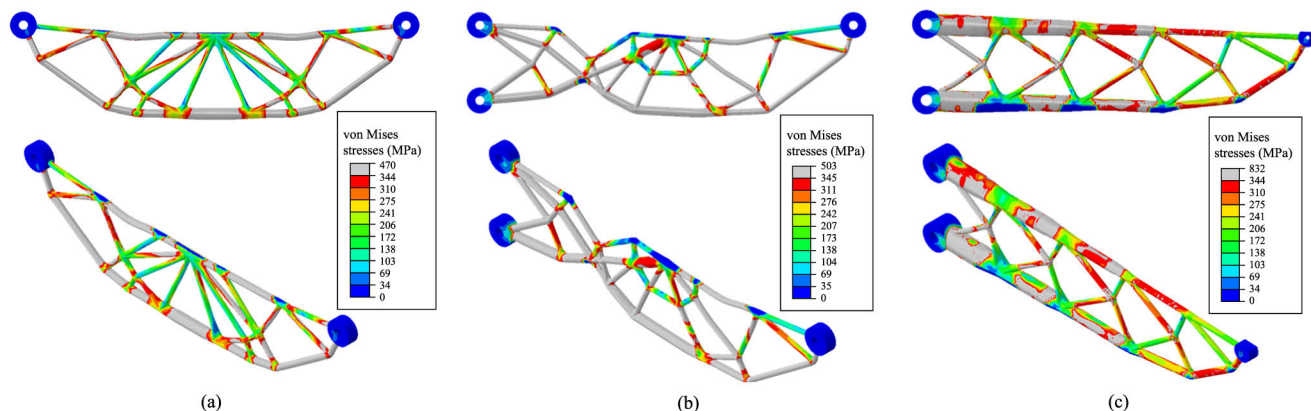
FIGURE 11. Deformed shapes and von Mises stress distributions for: (a) simply supported, (b) propped cantilever, and (c) cantilever trusses at peak load.

The load-displacement curves for the three optimized trusses are presented in Figure 12, where the results of both types of analysis (i.e. GMNIA and MNA) are plotted and compared against the target design load levels used in the optimization. The results of the MNA are in close accordance with the target design load level for the optimization of all three trusses because neither make allowance for strain hardening. Note that there is no peak load (or subsequent drop) since geometric nonlinearity (i.e. buckling) is suppressed in MNA.

For the simply supported truss, shown in Figure 12(a), the peak load determined from the GMNIA surpassed the target design load level, with the additional capacity attributed to strain hardening. Regarding the propped cantilever and cantilever trusses, presented in Figure 12(b) and 12(c) respectively, the load carrying capacity determined by the GMNIA fell marginally below the target design load level used in the optimization process, implying that the imperfections and buckling effects in the FE models were slightly more severe than suggested by the considered member buckling design capacities, as given by Equation (4). Overall, however, in all three cases, the optimized trusses attained peak FE capacities that were close (within 7%) to the target values.

VII. EVALUATION OF OPTIMIZATION EFFICIENCY

The efficiency of the optimized trusses is assessed by comparing their performance against equivalent reference designs. Conventional beams were designed for the examined load case scenarios, with standard cross-sections selected from typical section tables provided by manufacturers. Comparisons between the optimization results and their corresponding reference designs (i.e. the hot-rolled S355 UB section with the lowest mass capable of carrying the applied load) are presented in Table 2, with ''opt'' and ''ref'' denoting the optimized and reference designs respectively. The capacity-to-mass ratio was in all cases found to be at least two times the equivalent ratio of the corresponding reference design. This suggests that the proposed optimization framework can

TABLE 2. Comparison of performance of optimized trusses against reference designs.

Truss	Target load P_1 (kN)	UB section	$\dfrac{\left(capacity/mass\right)_{opt}}{\left(capacity/mass\right)_{ref}}$
Simply supported	172	UB 203×133×25	2.13
Propped cantilever	246	UB 254×102×25	2.05
Cantilever	98	UB 305×127×42	2.24

be used to reduce material usage and improve structural performance.

VIII. ADDITIVE MANUFACTURING

Following evaluation of the optimization efficiency of the trusses, STL files with their final geometry were generated for additive manufacturing. The process followed for their manufacture is presented in this section.

The solid models of the optimized trusses presented in Section V were firstly modified to include only the middle surface of the optimized members and were then exported as STL files to be fed into the WAAM specific CAM software tool MetalXL employed by MX3D. The information regarding the thickness of the members is passed on by grouping the geometries in two layers depending on the desired output thickness – see Figure 13.

The build-up sequence of each truss was then determined. As shown in Figure 14(a), geometric features that are repeated and can be manufactured using the same printing strategy, these were identified and then grouped into broader zones of similar build sequence – see Figure 14(b). Given that, during AM, the position of the printing substrate needs to be changed to maintain the overhangs as close as possible to the vertical position at any given time, efficient planning of the print sequence is required to minimise the
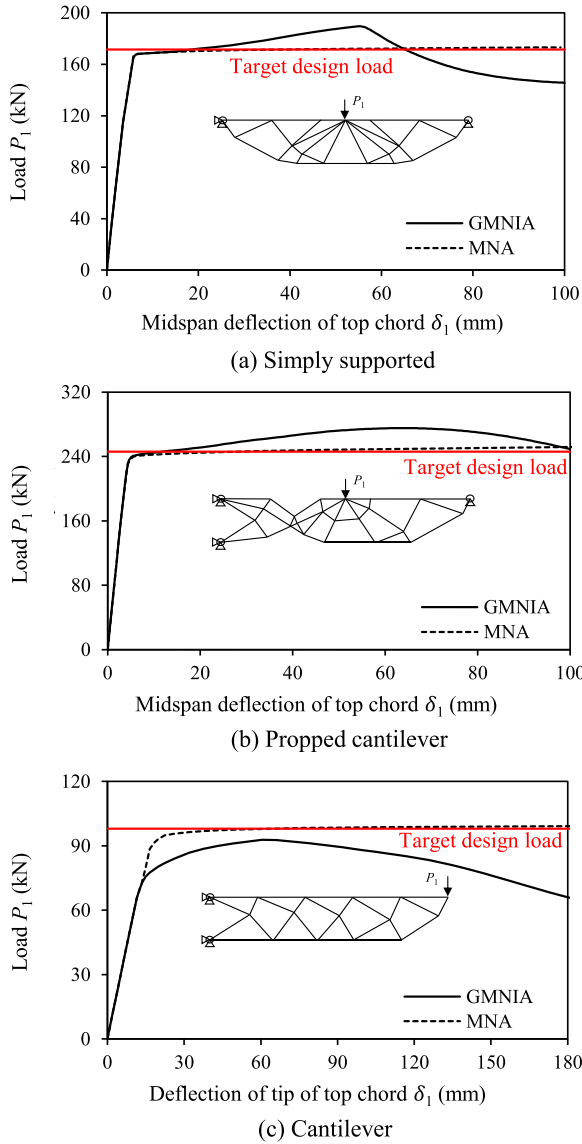
(a) Simply supported

(b) Propped cantilever

(c) Cantilever

FIGURE 12. Load-deflection curves of: (a) simply supported, (b) propped cantilever, and (c) cantilever trusses.
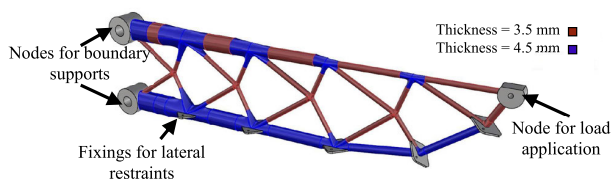

FIGURE 13. STL file of middle surface of cantilever truss with different thicknesses denoted by different layers.

FIGURE 14. Grouping of cantilever truss members: (a) 3 types of connections and (b) 5 building zones.

FIGURE 15. Visualisation of: (a) different segments of a typical joint and the consequent layer orientation and (b) the torch approach position on one of the segments.

required amount of substrate reorientation, while maintaining the growth of the geometry as levelled as possible. Therefore, further subdivision of the CAD file of each truss into smaller truss segments was performed to tackle the steepest overhangs while avoiding collisions between the AM parts
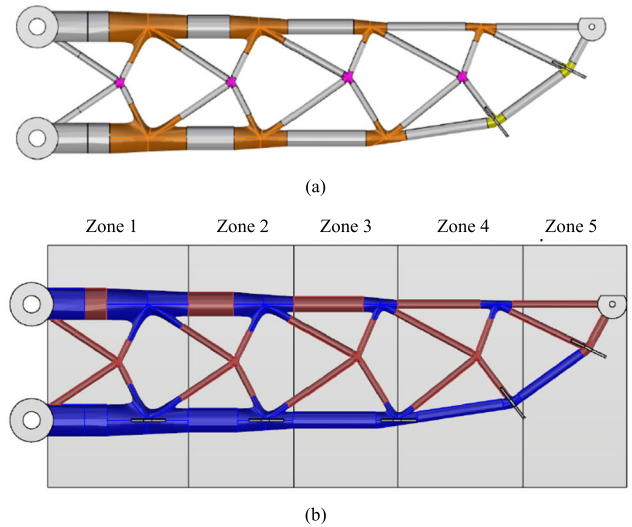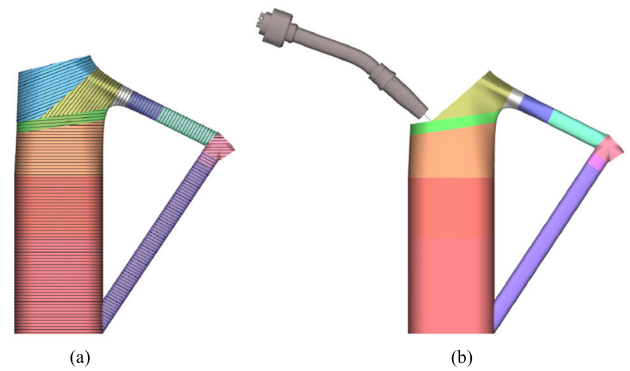
and the welding machine. A typical subdivision of one of the truss joints and the consequent layer direction are shown in Figure 15(a). Note that the geometry of the welding torch is used as a constraint for the reorientation and splitting angle used – see Figure 15(b).

Finally, to ensure that execution of the selected printing process was feasible, all steps of the printing sequence were simulated in the virtual environment of Metal XL using slicing and kinematic analysis. The former type of analysis generates the tracks and targets that represent the motion plan for the robot to guide the WAAM tool during the deposition process, while the latter calculates the correct joint orientation of the robotic system to correctly move the end effector (i.e. the deposition tool) through the motion plan without running into limitations due to mechanical constraints. While processing the tool path, singularities and movements that are beyond the joint boundaries are avoided as such actions would disrupt the motion planning. Once the simulation of
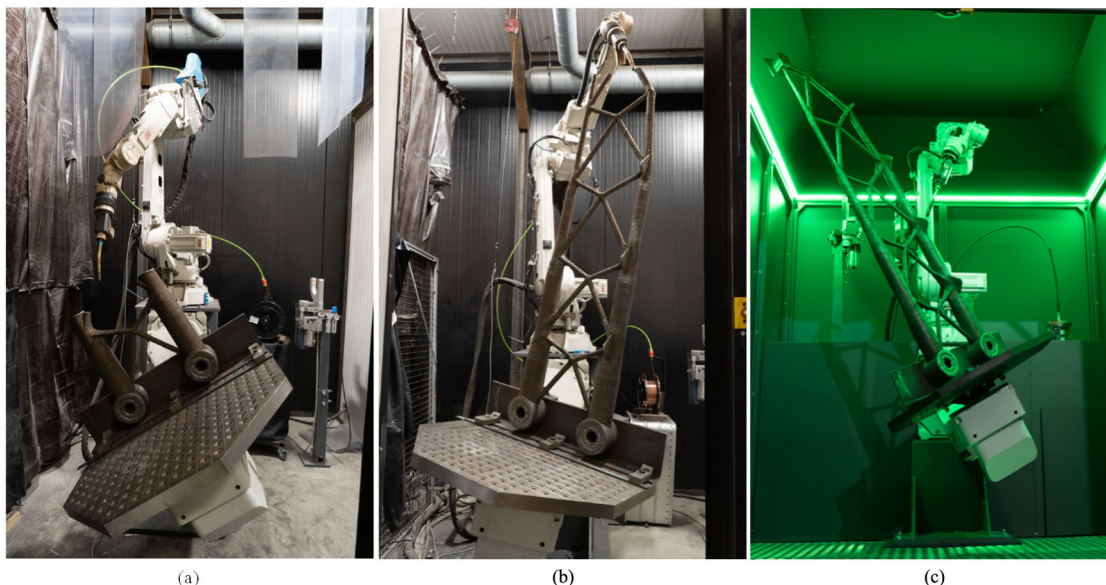
FIGURE 16. Printing of the cantilever truss: (a) zone 1, (b) zones 1 - 4 and (c) full truss.

the entire print sequence was validated, the machine code was generated and queried for printing. AM of the truss was then initiated, starting from zone 1, as per Figure14(b), and up to zone 5. Typical phases of the printing process for the cantilever truss are shown in Figure 16.

IX. INSPECTION

The final step of the proposed framework, described in this section, is the inspection and quality control of the AM trusses. To ensure prints of high quality, several methods ranging from inline quality monitoring to visual inspection were employed, both during and after the printing cycle.

A sophisticated sensor network bundled into an integrated online control system was used to monitor the most critical printing parameters – mainly the voltage and current – during AM at a high frequency. The interpass temperature was controlled through an IR sensor placed next to the deposition tool. The sensor data were monitored in real time in the software solution MetalLive as curve functions, as shown in Figure 17(a). The data logs can be inspected further using the offline visualisation tool MetalLive, using specific colour gradients applied to each printed track, for the operator to have a global view of the part build-up – see Figure 17(b). The system is designed to halt the process and alert the operator whenever specific variable fluctuations are detected, such as large fluctuations in the distance between the electrode and the substrate, a wrong interpass temperature or significant discrepancies from the average voltage and current that might be attributed to dirt, defects or uneven deposition.

Visual inspection of the most critical parts of the print should also be carried out. If necessary, the operator can enter the printing cell and, with increased safety measures, prevent potential defects by following specific mitigation
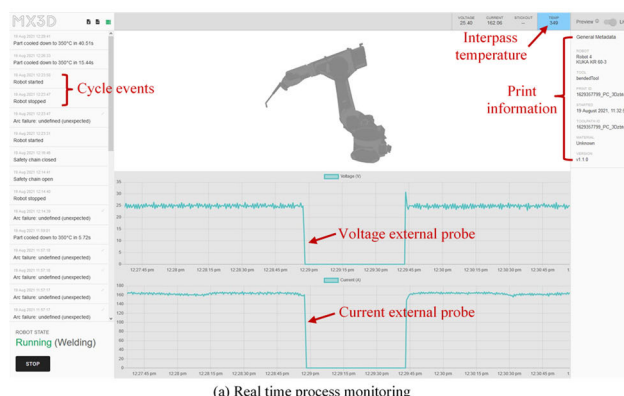
(a) Real time process monitoring
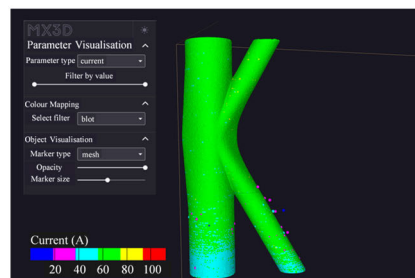
(b) Colour monitoring of current

FIGURE 17. Logging system during WAAM.

steps, such as cleaning the welding torch, changing worn-out consumables, levelling the layer with the use of a grinding disc and cutting off portions of the print that are considered of poor quality. Following completion of printing, the trusses were sandblasted to remove any welding soot from the WAAM process (see Figures 18(a) and 18(b) for the cantilever truss before and after sandblasting respectively)

FIGURE 18. Cantilever truss (a) before and (b) after sandblasting.

and the final visual inspection was conducted. In case any small defects (e.g. cracks, small pores etc.) are detected, the affected area can be cleaned with a grinding disc and filled with conventional welding.

X. CONCLUSION

An end-to-end framework has been introduced for the optimization and WAAM of structural elements, accounting for both manufacturing and practical constraints. Layout and geometry optimization methods were used to determine the topology of the optimized elements while cross-sectional optimization was also undertaken to obtain circular tubular cross-sections conforming to the WAAM constraints. Integrated connections were also generated through a series of geometric operations. The resulting geometric model was exported for additive manufacturing. The printing sequence was determined and the feasibility of its execution was validated. During the WAAM process, the critical printing parameters were monitored and controlled, while visual inspection of the finalised truss was also undertaken.

The structural performance of the optimized designs was assessed by means of FE analysis. Sophisticated FE models were developed, accounting for geometric and material nonlinearities and validated against physical experiments reported in the literature. Following their validation, the FE models were employed to examine the response of the optimized trusses; comparisons were then made with equivalent conventional reference designs. The structural efficiency of each optimized structures (as measured by the capacity-to-mass ratio) was found to be at least two times that of the corresponding reference design, confirming the effectiveness of the proposed optimization framework.

REFERENCES

[1] C. Buchanan and L. Gardner, "Metal 3D printing in construction: A review of methods, research, applications, opportunities and challenges," *Eng. Struct.*, vol. 180, pp. 332–348, Feb. 2019.

[2] R. A. Buswell, R. C. Soar, A. G. F. Gibb, and A. Thorpe, "Freeform construction: Mega-scale rapid manufacturing for construction," *Autom. Construct.*, vol. 16, no. 2, pp. 224–231, Mar. 2007.

[3] S. W. Williams, F. Martina, A. C. Addison, J. Ding, G. Pardal, and P. Colegrove, "Wire + arc additive manufacturing," *Mater. Sci. Technol.*, vol. 32, no. 7, pp. 641–647, Feb. 2016.

[4] C. Buchanan, V.-P. Matilainen, A. Salminen, and L. Gardner, "Structural performance of additive manufactured metallic material and cross-sections," *J. Construct. Steel Res.*, vol. 136, pp. 35–48, Sep. 2017.

[5] J.-J. Yan, M.-T. Chen, W.-M. Quach, M. Yan, and B. Young, "Mechanical properties and cross-sectional behavior of additively manufactured high strength steel tubular sections," *Thin-Walled Struct.*, vol. 144, Nov. 2019, Art. no. 106158.

[6] L. Gardner, P. Kyvelou, G. Herbert, and C. Buchanan, "Testing and initial verification of the world's first metal 3D printed bridge," *J. Construct. Steel Res.*, vol. 172, Sep. 2020, Art. no. 106233.

[7] MX3D. *About—MX3D*. Accessed: Sep. 1, 2020. [Online]. Available: https://mx3d.com/

[8] O. Sigmund, "A 99 line topology optimization code written in MATLAB," *Struct. Multidisciplinary Optim.*, vol. 21, no. 2, pp. 120–127, Apr. 2001.

[9] M. Gilbert and A. Tyas, "Layout optimization of large-scale pin-jointed frames," *Eng. Comput.*, vol. 20, no. 8, pp. 1044–1064, Dec. 2003.

[10] C. J. Smith, M. Gilbert, I. Todd, and F. Derguti, "Application of layout optimization to the design of additively manufactured metallic components," *Struct. Multidisciplinary Optim.*, vol. 54, no. 5, pp. 1297–1313, Apr. 2016.

[11] L. He and M. Gilbert, "Rationalization of trusses generated via layout optimization," *Struct. Multidisciplinary Optim.*, vol. 52, no. 4, pp. 677–694, Jul. 2015.

[12] L. He, M. Gilbert, T. Johnson, and T. Pritchard, "Conceptual design of AM components using layout and geometry optimization," *Comput. Math. With Appl.*, vol. 78, no. 7, pp. 2308–2324, Oct. 2019.

[13] C. Huang, P. Kyvelou, R. Zhang, B. T. Britton, and L. Gardner, "Mechanical testing and microstructural analysis of wire arc additively manufactured carbon steels," *Mater. Des.*, to be published.

[14] V. Laghi, M. Palermo, L. Tonelli, G. Gasparini, L. Ceschini, and T. Trombetti, "Tensile properties and microstructural features of 304L austenitic stainless steel produced by wire-and-arc additive manufacturing," *Int. J. Adv. Manuf. Technol.*, vol. 106, nos. 9–10, pp. 3693–3705, Jan. 2020.

[15] P. Kyvelou, H. Slack, D. D. Mountanou, M. A. Wadee, T. B. Britton, C. Buchanan, and L. Gardner, "Mechanical and microstructural testing of wire and arc additively manufactured sheet material," *Mater. Des.*, vol. 192, Jul. 2020, Art. no. 108675.

[16] P. Kyvelou, C. Huang, L. Gardner, and C. Buchanan, "Structural testing and design of wire arc additively manufactured square hollow sections," *J. Struct. Eng.*, vol. 147, no. 12, Dec. 2021, Art. no. 04021218.

[17] N. Hadjipantelis, B. Weber, C. Buchanan, and L. Gardner, "Description of anisotropic material response of wire and arc additively manufactured thin-walled stainless steel elements," *Thin-Walled Struct.*, vol. 171, Feb. 2022, Art. no. 108634.

[18] X. Guo, P. Kyvelou, J. Ye, L. H. Teh, and L. Gardner, "Testing and analysis of wire arc additively manufactured steel single lap shear bolted connections," *Eng. Struct.*, to be published.

[19] R. McNeel. (2010). *Grasshopper Generative Modeling for Rhino*. [Online]. Available: http://www grasshopper3dcom

[20] O. Zhao, L. Gardner, and B. Young, "Testing and numerical modelling of austenitic stainless steel CHS beam–columns," *Eng. Struct.*, vol. 111, pp. 263–274, Mar. 2016.

[21] X. Lan, J. Chen, T.-M. Chan, and B. Young, "The continuous strength method for the design of high strength steel tubular sections in bending," *J. Construct. Steel Res.*, vol. 160, pp. 499–509, Sep. 2019.

[22] X. Meng and L. Gardner, "Cross-sectional behaviour of cold-formed high strength steel circular hollow sections," *Thin-Walled Struct.*, vol. 156, Nov. 2020, Art. no. 106822.

[23] O. Zhao, B. Rossi, L. Gardner, and B. Young, "Behaviour of structural stainless steel cross-sections under combined loading—Part I: Experimental study," *Eng. Struct.*, vol. 89, pp. 236–246, Apr. 2015.

[24] *Eurocode 3: Design of Steel Structures. Part 1–1: General Rules and Rules for Buildings*, Standard EN 1993-1-1, European Committee for Standardization (CEN), Brussels, Belgium, 2005.

[25] D. W. A. Rees, *Mechanics of Optimal Structural Design: Minimum Weight Structures*. Hoboken, NJ, USA: Wiley, 2009.

[26] *MATLAB*, MathWorks, Natick, MA, USA, 2012.

[27] R. McNeel. (2015). *Rhinoceros. NURBS Modeling for Windows*. [Online]. Available: http://www. rhino3d.com/jewelry.Htm

[28] *ABAQUS, CAE User's Manual*, Dassault Systèmes Simulia Corp., USA, 2016.

[29] V.-A. Silvestru, I. Ariza, J. Vienne, L. Michel, A. M. A. Sanchez, U. Angst, R. Rust, F. Gramazio, M. Kohler, and A. Taras, "Performance under tensile loading of point-by-point wire and arc additively manufactured steel bars for structural components," *Mater. Des.*, vol. 205, Jul. 2021, Art. no. 109740.

[30] X. Yun and L. Gardner, "Stress-strain curves for hot-rolled steels," *J. Construct. Steel Res.*, vol. 133, pp. 36–46, Jun. 2017.

[31] H. Wu, C. Zhang, B.-Q. Gao, and J. Ye, "Theoretical and experimental study of robustness based design of single-layer grid structures," *Struct. Eng. Mech.*, vol. 52, no. 1, pp. 19–33, Oct. 2014.

JUN YE was born in Hubei, China, in 1987. He received the B.S. degree in civil engineering from Wuhan University, in 2010, the M.S. degree in structural engineering from Zhejiang University, in 2013, and the Ph.D. degree in structural engineering with The University of Sheffield, in 2016.

From 2016 to 2021, he was a Research Associate with the University of Bath and Imperial College London. Since 2021, he has been a Lecturer (Assistant Professor) in structural engineering with the University of Strathclyde, Glasgow, U.K., and a Professor in structural engineering with Zhejiang University, China. He has authored more than 30 journal articles. His research interests include steel structural design, digital structural design, and smart structures.

Dr. Ye is a member of the Institution of Engineering and Technology, U.K., and a First Class Registered Structural Engineer in China.

PINELOPI KYVELOU received the M.Sc. degree in earthquake engineering from Imperial College London, the Diploma degree in civil engineering from the National Technical University of Athens, and the Ph.D. degree in structural engineering from Imperial College London, in 2017.

She is currently a Research Associate with the Department of Civil and Environmental Engineering, Imperial College London, and an Affiliated Member of the Alan Turing Institute. She is engaged in teaching at both undergraduate and postgraduate level and she has co-supervised a number of Ph.D., M.Sc., and undergraduate students. Her research interests include the areas of testing, numerical modeling and development of design guidance for metallic 3D printed structural members and composite cold-formed steel systems, on which she has coauthored several technical papers. She is a member of the Institution of Structural Engineers, U.K., and a Chartered Member of the Technical Chamber of Greece.

FILIPPO GILARDI was born in Sondrio, Italy, in 1988. He received the B.S. degree in industrial design and the M.Sc. degree in industrial design for process innovation from the Politecnico di Milano, Italy.

From 2013 to 2015, he worked as a Researcher and a Developer of innovative production methods for the Joris Laarman Lab, focusing mainly on the application of CNC technologies on generative design. Since 2015, he has been leading the Department of Research and Development, MX3D, a major player in Robotic WAAM Technology and Services based in Amsterdam, The Netherlands. In 2018, he and his colleagues earned their badge of honor by creating the first 3D printed steel bridge in the world, a 12 meter/6 ton stainless steel bridge for the city center of Amsterdam. Since then, he has focused on many innovative projects, helping to consolidate WAAM technology by bringing it to the forefront of the most demanding industries. He has contributed to many scientific papers and publications regarding the application of robotic WAAM in different industrial fields, often focused on structural optimization, parametric design, and disruptive applications. His research interests include WAAM for infrastructure and civil engineering.

HONGJIA LU was born in Jiangsu, China, in 1991. He received the B.Eng. degree in civil engineering from the University of Liverpool, in 2013, the M.Sc. degree in general structural engineering from Imperial College London, in 2014, and the Ph.D. degree in structural optimization from The University of Sheffield, in 2017.

From 2017 to 2019, he was a Software Developer at LimitState Ltd. Since 2019, he has been a Research Associate with The University of Sheffield. His research interests include building structure optimization and the application of structural optimization in additive manufacturing.

MATTHEW GILBERT was born in Hull, East Yorkshire, U.K., in 1968. He received the B.Eng. degree in civil and structural engineering from The University of Sheffield, U.K., in 1989, and the Ph.D. degree in civil engineering from The University of Manchester, U.K., in 1993.

Since 1993, he has held research and academic positions at the Department of Civil and Structural Engineering, The University of Sheffield, U.K., where he has been holding the position of a Professor, since 2013. He holds one patent. His longstanding research interest includes the area of structural optimization.

Prof. Gilbert has been a Chartered Member of the Institution of Civil Engineers, since 2000. He was a recipient of prizes for published papers awarded by the Institution of Civil Engineers and the Institution of Structural Engineers. He has also coauthored a paper awarded the 2011 Springer Prize by the International Society for Structural and Multidisciplinary Optimization. He is an Honorary Editor of the Institution of Civil Engineers Proceedings journal *Engineering and Computational Mechanics* and a Review Editor of the journal *Structural and Multidisciplinary Optimization*.

LEROY GARDNER was appointed as a Distinguished Visiting Professor at Tsinghua University, in 2018. He is currently a Professor of structural engineering at Imperial College London and a fellow of the Royal Academy of Engineering. He is engaged in teaching at both undergraduate and postgraduate level, industry training, and specialist advisory work, and leading an active research group in structural engineering. His principal research interests include the testing, simulation, analysis, design, and construction of steel structures, on which he has coauthored four textbooks, seven book chapters, and over 400 technical papers.

Prof. Gardner was awarded the IABSE Prize, in 2017, and the ASCE Shortridge Hardesty Award, in 2021. He is the Editor-in-Chief of two international journals and serves on a number of code committees in Europe and USA.

• • •